

Thermodynamic, magnetic, and transport properties of the repulsive Hubbard model on the kagome lattice

Andressa R. Medeiros-Silva ^{1,2}, Natanael C. Costa ¹, and Thereza Paiva ¹

¹*Instituto de Física, Universidade Federal do Rio de Janeiro, Rio de Janeiro, Rio de Janeiro 21941-972, Brazil*

²*Departamento de Física, Universidade Federal do Piauí, 64049-550 Teresina, Piauí, Brazil*



(Received 2 September 2022; revised 6 December 2022; accepted 6 January 2023; published 20 January 2023)

Over the past few decades, magnetic frustration has been under intense debate due to its unusual properties. For instance, frustration in the kagome lattice suppresses long-range spin correlations, and it is expected to be a candidate for a spin liquid system. Therefore, with the advent of experiments with ultracold atoms, the interest in frustrated geometries has increased. Given this, in the present work we investigate the repulsive Hubbard model on the kagome lattice using unbiased quantum Monte Carlo simulations. We examine its thermodynamic properties, as well as the magnetic and transport response of the system at finite temperatures and different values of the repulsive interaction. From these results, we discuss the possible occurrence of adiabatic cooling, a quite important feature in ultracold systems, and the presence of a metal-to-insulator transition at a finite interaction strength. Our findings may guide future experiments in ultracold fermionic atoms on the kagome lattice.

DOI: [10.1103/PhysRevB.107.035134](https://doi.org/10.1103/PhysRevB.107.035134)

I. INTRODUCTION

Magnetic frustration is a central issue in condensed matter physics, with great experimental effort being devoted, over the past few decades, to understanding its effects. Indeed, the interest comes from the emergence of a myriad of correlated phases at low temperatures due to the highly degenerate ground state of such systems. Among the many geometries leading to frustration, the kagome lattice (see Fig. 1) has gained much attention recently due to the possibility of the occurrence of a quantum spin liquid (QSL) state. The experimental realization of this geometry is found, e.g., in herbertsmithite compounds [1,2], exhibiting strong evidence for the occurrence of QSL, although its nature is still under debate [3–5]. The electronic properties of the kagome lattice have also been investigated by the manipulation of atoms and molecules on given substrates [6,7], although the tuning of the interaction strength remains a challenge. The advent of optical lattices has raised great expectations for unveiling fundamental properties of strongly correlated systems, in particular those with frustration. Within this context, optical lattices for the kagome geometry were recently realized for bosonic atoms [8–10], and one expects that fermionic ones could be realized in the near future. In spite of the experimental effort, manipulating these many-body states is an arduous task; therefore, providing information that could guide experiments is clearly in order.

From a theoretical point of view, the ground state properties of the Heisenberg model in the kagome lattice have been extensively examined, with the nature of its QSL phase (gapped or gapless) being a matter under debate [11,12]. However, this picture is less clear for the half-filled Hubbard model: many studies, using different techniques, agree on the occurrence of a Mott transition from a finite value of interac-

tion, although controversies on the critical value remain. For instance, by using variational cluster approximation, Yamada *et al.* [13] examined the occurrence of a metal-to-insulator transition as the interaction strength increased, finding a critical point at $U_c/t \approx 5$, while Higa and Asano [14] suggested that such a transition should occur at $U_c/t = 6.8$. Similarly, Ohashi *et al.* [15] found this Mott transition around $U_c/t = 8.22$, using cellular dynamical mean-field theory, while variational Monte Carlo studies, conducted by Kuratani *et al.* [16], exhibit $U_c/t \approx 11$. The lack of a consensus about U_c in these studies may be due to the particularities of their implementations, i.e., due to the way their biased input is added and how it improves their ground states.

Unbiased methodologies are usually limited by technical issues, as the fermionic minus-sign problem for quantum Monte Carlo (QMC) approaches, or by dimensionality for the density-matrix renormalization group (DMRG). Early attempts to perform finite-temperature determinant QMC (DQMC) simulations were conducted by Bulut *et al.* [17], without clear evidence for a Mott transition. Recently, by combining dynamical vertex approximation, dynamical mean-field theory, and DQMC, Kaufmann *et al.* [18] further examined how the magnetic correlation evolves in the kagome lattice and proposed a critical point within a range of $U_c/t = [7, 9]$. On the other hand, DMRG results [19] provide evidence for two critical points, one for a translational-symmetry-broken insulator and the other one for a QSL, at $U_{c1}/t \approx 5.4$ and $U_{c2}/t \approx 7.9$, respectively. Away from half filling physical responses are even less clear, with the enhancement of unconventional pairing correlations [20].

Despite these recent advances, many of the thermodynamic properties of the Hubbard model in the half-filled kagome lattice are unknown. Knowing the many different energy scales of the system is particularly important in cold atoms

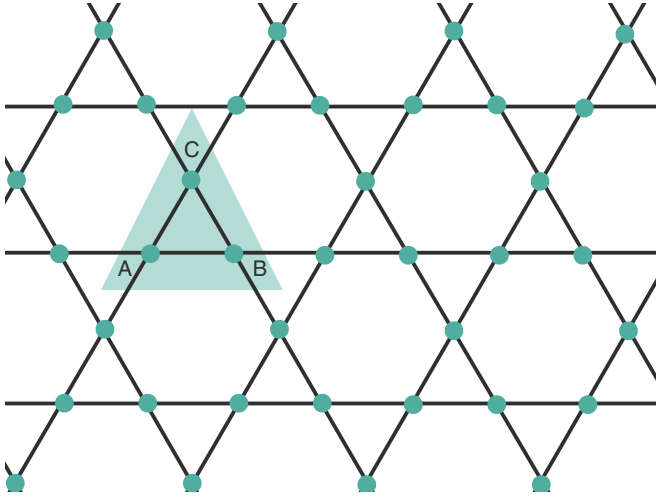


FIG. 1. The kagome lattice. The highlighted triangle describes the unit cell with its A, B, and C basis sites.

experiments. In order to bridge this gap, in this work we perform a *tour de force* using the DQMC method to examine the thermodynamic, magnetic, and transport properties of such a frustrated system. These analyses allow us to show the critical point within some accuracy and also unveil hints about the ground state properties [21]. This paper is organized as follows. In Sec. II we present the main features of the Hubbard Hamiltonian and highlight the DQMC method together with the quantities of interest. The results are presented in Sec. III, in which we discuss the thermodynamic, magnetic, and transport properties. Our main conclusions are then summarized in Sec. IV.

II. MODEL AND METHODOLOGY

Here we investigate fermions under a repulsive on-site interaction, namely, the Hubbard model. Its symmetric Hamiltonian reads

$$\mathcal{H} = -t \sum_{\langle \mathbf{i}, \mathbf{j} \rangle, \sigma} (c_{\mathbf{i}\sigma}^\dagger c_{\mathbf{j}\sigma} + \text{H.c.}) - \mu \sum_{\mathbf{i}, \sigma} n_{\mathbf{i}, \sigma} + U \sum_{\mathbf{i}} (n_{\mathbf{i}, \uparrow} - 1/2)(n_{\mathbf{i}, \downarrow} - 1/2), \quad (1)$$

where the sums run over sites of the kagome lattice, with $\langle \mathbf{i}, \mathbf{j} \rangle$ denoting nearest-neighbor sites under periodic boundary conditions. In Eq. (1), we use the second quantization formalism, with $c_{\mathbf{i}\sigma}^\dagger$ ($c_{\mathbf{i}\sigma}$) being creation (annihilation) operators of electrons on a given site \mathbf{i} and spin σ , while $n_{\mathbf{i}\sigma} \equiv c_{\mathbf{i}\sigma}^\dagger c_{\mathbf{i}\sigma}$ are number operators. The first two terms on the right-hand side of the Hamiltonian correspond to the hopping of fermions and the chemical potential μ , respectively, with the latter determining the filling of the bands. The third term describes the local repulsive interaction between fermions, with coupling strength U . Hereafter, we define the lattice constant as unity and the hopping integral t as the energy scale.

We investigate the thermodynamic properties of Eq. (1) on the half-filled kagome lattice by performing DQMC simulations [22–25]. The DQMC method is an unbiased numerical approach which maps a many-particle

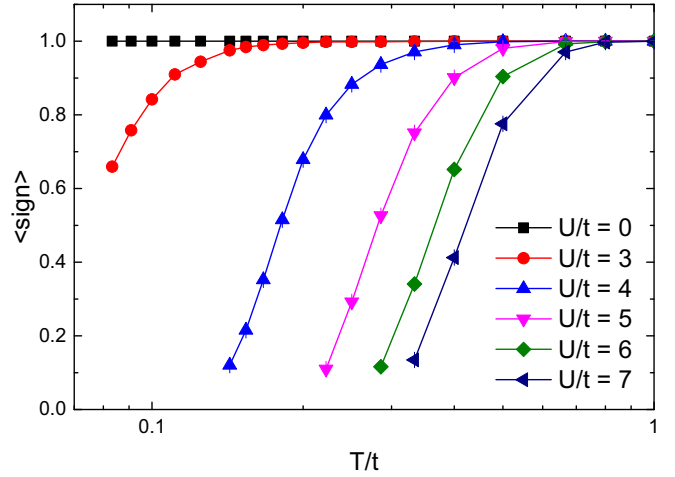


FIG. 2. The average fermionic sign as a function of the temperature for different values of U/t . When not shown, error bars are smaller than the symbol size.

interacting fermionic system into a single-particle (quadratic form) one, with the aid of bosonic auxiliary fields. In summary, the method separates the exponentials of the one-body and two-body terms, $\hat{\mathcal{K}}$ and $\hat{\mathcal{P}}$, respectively, in the partition function by performing a Trotter-Suzuki decomposition, i.e., $\mathcal{Z} = \text{Tr} e^{-\beta \hat{\mathcal{H}}} = \text{Tr} [(e^{-\Delta\tau(\hat{\mathcal{K}} + \hat{\mathcal{P}})})^{L_\tau}] \approx \text{Tr} [e^{-\Delta\tau \hat{\mathcal{K}}} e^{-\Delta\tau \hat{\mathcal{P}}} e^{-\Delta\tau \hat{\mathcal{K}}} e^{-\Delta\tau \hat{\mathcal{P}}} \dots]$. Here $L_\tau = \beta/\Delta\tau$ is the size of the imaginary-time coordinate, corresponding to the number of incremental time evolution operators, with the inverse temperature $\beta \equiv 1/(k_B T)$, where k_B is the Boltzmann constant. Such a decomposition has an error proportional to $(\Delta\tau)^2$, being exact in the limit $\Delta\tau \rightarrow 0$. In this work, we choose $t\Delta\tau \leq 0.05$, so that the error from the Trotter-Suzuki decomposition is negligible compared to that from the Monte Carlo sampling.

Proceeding, we perform a discrete Hubbard-Stratonovich transformation to rewrite quartic operators into quadratic (single-particle) ones, but at the cost of introducing auxiliary fields $s(\mathbf{i}, \tau)$ on both real- and imaginary-time coordinates, which are sampled by the regular Monte Carlo techniques. Finally, from the Green's function and by using Wick contractions, all the higher-order correlation functions may be obtained. More details about this methodology are discussed in Refs. [26–29] and references therein.

III. RESULTS

A. Sign and the half filling

Although it is an unbiased methodology, DQMC suffers the infamous minus-sign problem, leading to noisy averages [30,31]. This problem does not exist in half-filled systems with particle-hole symmetry (PHS), such as bipartite lattices like the square and honeycomb ones. However, the kagome lattice is nonbipartite, and there is no PHS for any filling, which, in turn, may lead to a severe the sign problem depending on the system size, temperature scale, and interaction strength. To further illustrate the sign problem, Fig. 2 shows the average sign as a function of temperature T/t at half filling

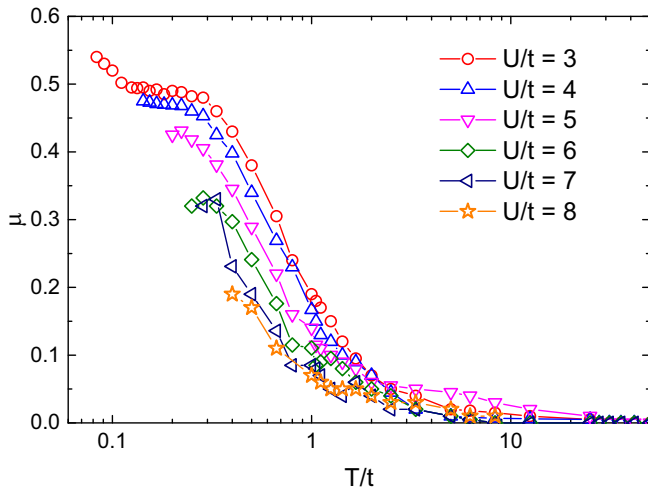


FIG. 3. The chemical potential that leads to the half filling of the system as a function of the temperature for different values of interaction strengths.

on the kagome lattice for different U/t values and for the fixed linear size $L = 6$, i.e., $N = 6 \times 6 \times 3$ sites. Notice that the sign decreases as the temperature is lowered, and it is strongly suppressed as U/t increases (this behavior is more accentuated for larger system sizes). Therefore, the following results are obtained for $L = 6$, keeping $\langle \text{sign} \rangle \gtrsim 0.05$, which, for some cases, demands simulations up to 5×10^6 Monte Carlo sweeps for measurements. Similarly, unless otherwise indicated, the results for the noninteracting case ($U/t = 0$) are obtained in the thermodynamic limit.

Another important feature of the kagome lattice is that, due to the absence of the PHS, half filling is not at $\mu = 0$. Therefore, one needs to vary the chemical potential in order to find which μ leads to $\langle n \rangle = 1$. Figure 3 shows how the chemical potential leading to a half-filled band at different U/t changes with temperature.

B. Thermodynamic properties

We start our analysis by discussing the thermodynamic properties of the system. First, we investigate the internal energy density,

$$e(\beta, U) = \frac{1}{N} \langle \mathcal{H} \rangle, \quad (2)$$

which is shown in Fig. 4(a). Given this, one is able to obtain the entropy per site (in units of the Boltzmann constant k_B) with [32]

$$s(\beta, U) = \ln 4 + \beta e(\beta, U) - \int_0^\beta e(\beta', U) d\beta', \quad (3)$$

which is shown in Fig. 4(b). As expected, we obtain $s(T \rightarrow \infty) \equiv \ln 4$ for all U/t , while it decreases and goes toward zero when T is reduced. However, the way $s(T) \rightarrow 0$ depends on the value of U/t . For instance, for $U/t = 3$, the entropy approaches zero in a way closely similar to that in the noninteracting case, while for $U/t = 7$ it decays slowly at low temperatures, directly affecting the specific heat, as discussed later.

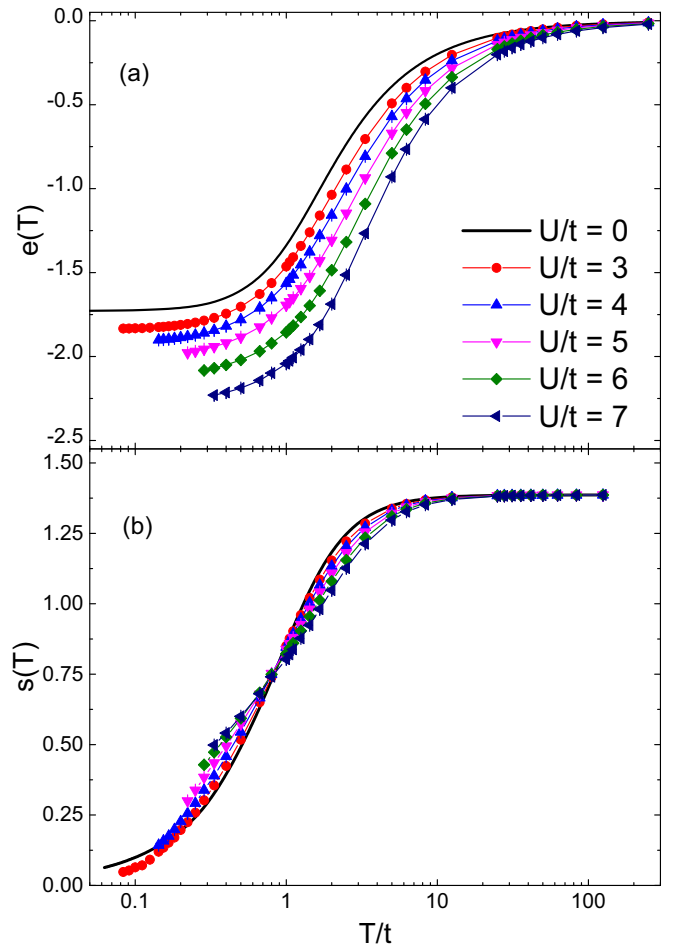


FIG. 4. The (a) total energy and (b) entropy as a function of the temperature for different values of U/t . When not shown, error bars are smaller than the symbol size.

Interestingly, the entropy curves for different values of the interaction strength cross around $s \approx \ln 2$. This crossing has also been observed for the square [33–36] and honeycomb [35–37] lattices and is closely connected to the possibility of adiabatic cooling in the system. That is, for entropies greater than $s \approx \ln 2$, Fig. 4(b) shows that increasing U/t (at fixed entropy) pushes the temperature up. On the other hand, below $s \approx \ln 2$, increasing U/t at fixed entropy actually cools the system. At this point, we recall that this change in behavior should occur around an energy scale where the entropy of a Fermi liquid state becomes lower than the limit of the Heisenberg model (i.e., of localized spin 1/2). At high temperatures, the latter exhibits weakly interacting spins, which, in turn, leads to a crossing of entropies around $s \approx \ln 2$.

The adiabatic cooling/heating of the systems is shown in Fig. 5, which was constructed by selecting fixed values of entropy in Fig. 4(b) and gathering the temperature for each U/t value. A comparison of the isentropic curves on the square [38], honeycomb [35], and kagome lattices is also presented and shows that, for low values of s , adiabatic cooling on the kagome lattice is at least as effective as that in the honeycomb lattice. Further evidence of the effectiveness of adiabatic cooling in the kagome lattice is presented below in the

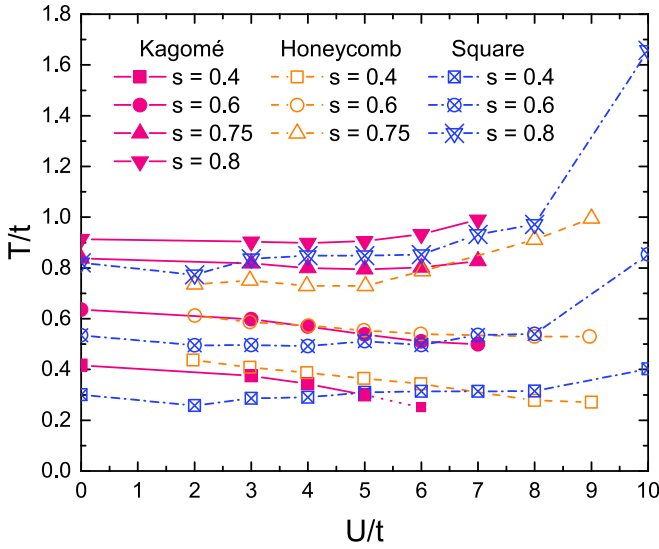


FIG. 5. Isentropic curves as a function of U/t for the kagome (solid symbols), honeycomb (open symbols), and square (crossed symbols) lattices.

investigation of the behavior of the double occupancy at lower temperatures.

Figures 6(a) and 6(b) display the behavior of the specific heat,

$$c(T) = \frac{1}{N} \frac{d\langle \mathcal{H} \rangle}{dT}, \quad (4)$$

for $U/t = 3$ and 6 , respectively. The data points correspond to the differentiation of the raw QMC results in Fig. 4(a), while the solid lines are obtained by differentiating a nonlinear fit of the energy; we use an exponential fit of the energy by the function $e_{\text{fit}}(T) = a_0 + \sum_{n=1}^M a_n \exp(-\beta n \Delta)$, with a cutoff at $M = 6$. Figure 6(c) presents the specific heat from the exponential fit for all values of U/t examined. For the noninteracting case, one notices the occurrence of a single peak around $T/t \approx 1$, which is pushed up to higher temperatures as U/t increases. Such a high-temperature broad peak is due to single-particle excitations and is closely related to the formation of local moments [33]. When the temperature is reduced, a soft shoulder appears for all $U > 0$, but without a large second peak, as displayed in Fig. 6(c). The occurrence of such a low-temperature peak is usually due to low-lying collective spin-wave excitations, with the double-peak structure indicating strong spin-spin correlations [33]. Interestingly, by employing a cellular dynamical mean-field theory approach, Udagawa and Motome [39] obtained a small second peak for the specific heat at low temperatures, which they suggested is related to spin chirality degrees of freedom. In view of these issues, we further investigate the magnetic properties of the Hubbard model in the kagome lattice in the next section.

C. Magnetic properties

Now, we turn our attention to the magnetic properties of the system, starting our analysis with the double occupancy,

$$D = \frac{1}{3L^2} \left\langle \sum_{i,\alpha} n_{i\uparrow} n_{i\downarrow} \right\rangle. \quad (5)$$

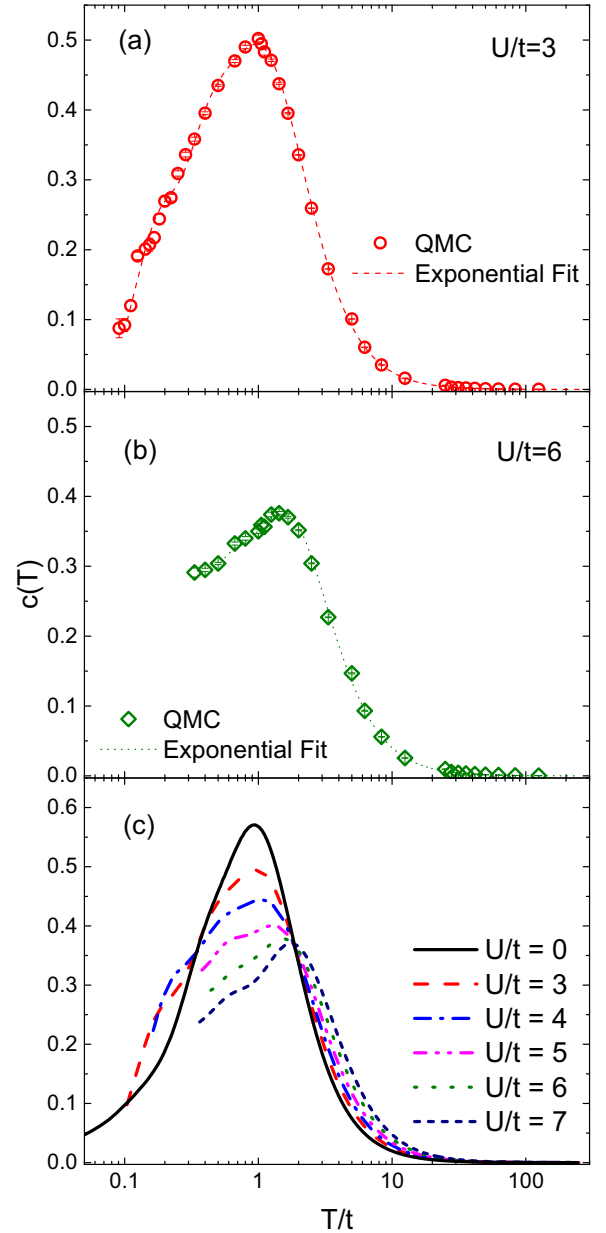


FIG. 6. The specific heat as a function of temperature for different values of U/t . The curves in (a) and (b) display a comparison between the numerical differentiation of the raw DQMC energy values and the differentiation of the exponential fit performed for $U/t = 3$ and $U/t = 6$, respectively. (c) The specific heat obtained from the exponential fit. When not shown, error bars are smaller than the symbol size.

The double occupancy and the local moment are connected by $D = \frac{1}{2}[\langle n \rangle - \langle m^2 \rangle]$; therefore, for fixed n , increasing the local moment reduces the double occupancy. Figure 7(a) displays D as a function of temperature for different values of U/t , where one can notice that D has a sharp decrease for $1 < T/t < 10$ with a minimum (for all values of U) around $T/t \lesssim 1$. This minimum suggests a competition between localization and delocalization of the fermions. As depicted in Fig. 7(b), when $T \rightarrow 0$, we find $\frac{\partial D}{\partial T} < 0$ for all U/t , a feature consistent with a metallic behavior. For $U/t = 7$, this

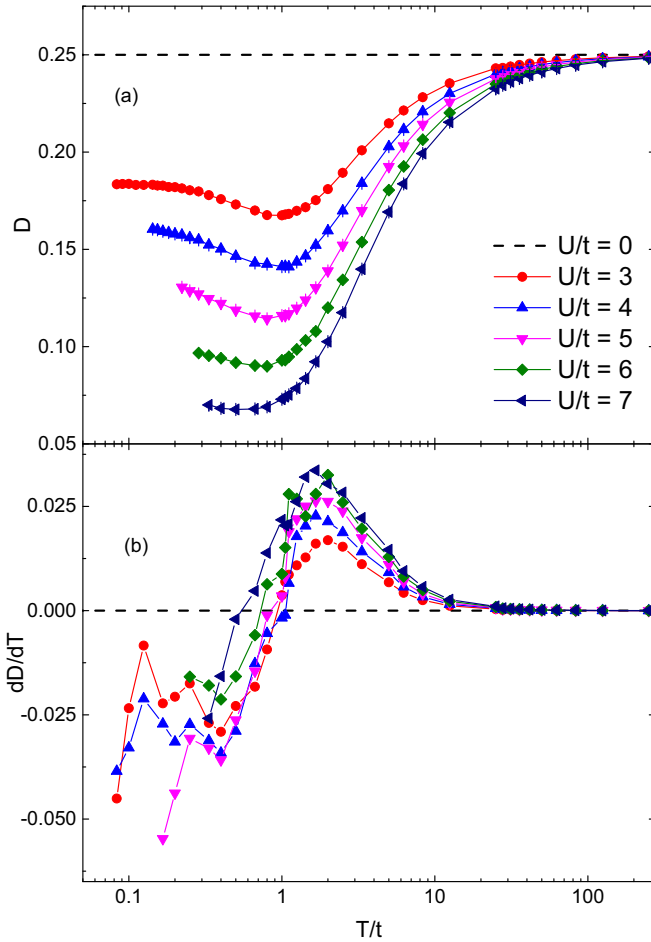


FIG. 7. (a) Double occupancy and (b) its derivative as a function of the temperature for different U/t . The derivatives were smoothed through the usual methods. When not shown, error bars are smaller than the symbol size.

minimum is shallow but has a large local moment, which suggests an insulating or bad metallic behavior. At this point it is worth mentioning that metallic or insulating behavior is closely connected to adiabatic cooling features. Indeed, since $(\frac{\partial D}{\partial T})_{N,U} = -(\frac{\partial S}{\partial U})_{N,T}$, when $(\frac{\partial S}{\partial U})_{N,T} > 0$ (in the adiabatic cooling region), $(\frac{\partial D}{\partial T})_{N,U} < 0$, which is consistent with a Fermi liquid at lower temperatures.

We proceed by probing nonlocal spin-spin correlation functions

$$c^{\alpha\gamma}(\mathbf{i} - \mathbf{j}) = \frac{1}{3} \langle \vec{S}_{\mathbf{i},\alpha} \cdot \vec{S}_{\mathbf{j},\gamma} \rangle, \quad (6)$$

with $\vec{S}_{\mathbf{i},\alpha} = (S_{\mathbf{i},\alpha}^x, S_{\mathbf{i},\alpha}^y, S_{\mathbf{i},\alpha}^z)$ being the spin operator of a fermion in given unit cell \mathbf{i} and site index $\alpha = A, B$, and C . We first explore the nearest-neighbor case $c(1)$, when $|\mathbf{i} - \mathbf{j}| = a$ (lattice parameter), i.e., the spin-spin correlations between the pairs of sites that form a triangle (see Fig. 1). Figure 8(a) shows $c(1)$ averaged over all the combinations of near-neighbor pairs in the lattice. $c(1)$ is negative and increases in magnitude as U/t increases; that is, there are strong spin-spin correlations along the sides of the triangle.

On the other hand, spin correlations for longer distances are suppressed, as displayed in Fig. 8(b) for next-nearest neighbors

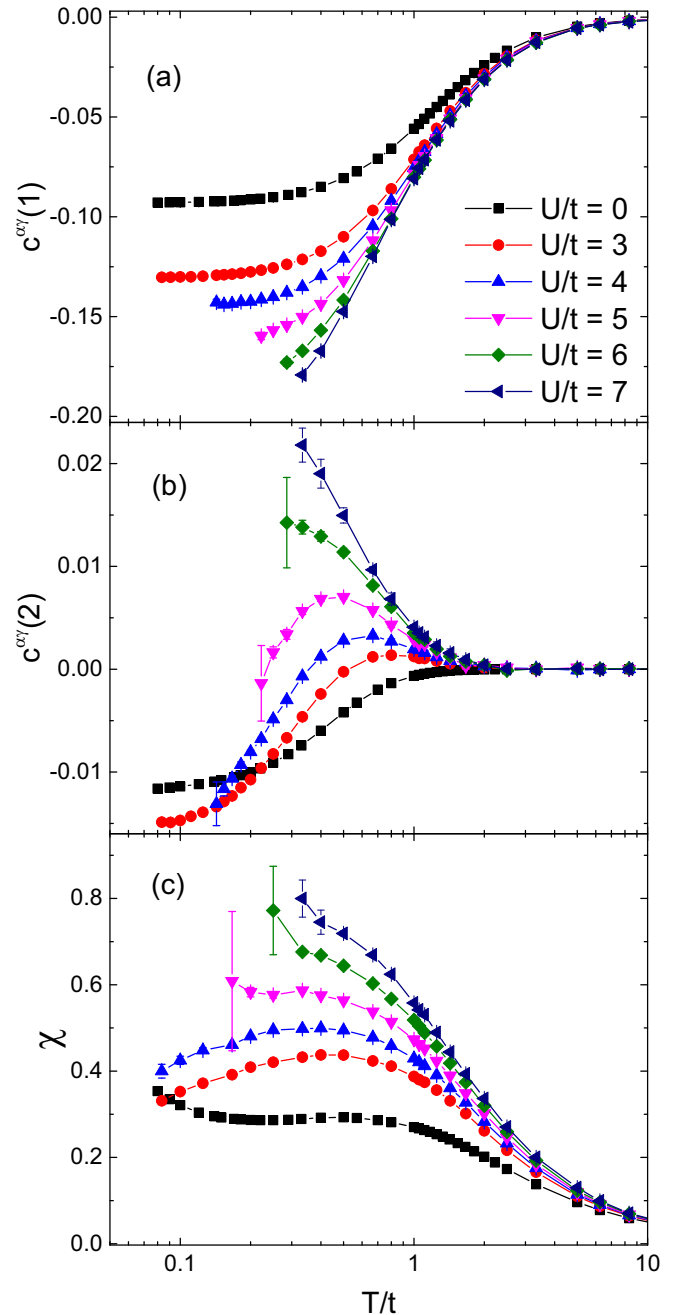


FIG. 8. The spin-spin correlation between (a) nearest neighbors, (b) next-nearest neighbors, and (c) the homogeneous magnetic susceptibility as a function of temperature for different values of U/t . When not shown, error bars are smaller than the symbol size.

neighbors [$c(2)$, when $|\mathbf{i} - \mathbf{j}| = 2a$], presenting values one order of magnitude smaller than those for $c(1)$. For $U/t \leq 4$ and at low temperatures, i.e., below the energy scale for local moment formation ($T/t \lesssim 2$), $c(2)$ is reduced to values very close to those of the noninteracting case, in line with a nonmagnetic state. Interestingly, for larger values of U , as for $U/t \geq 5$, $c(2)$ exhibits ferromagnetic correlations at high temperatures, and the effects of frustration (antiferromagnetic correlations) set in only for lower T/t . Finally, Fig. 8(c) displays the homogeneous susceptibility as a function of temperature. For $U/t \lesssim$

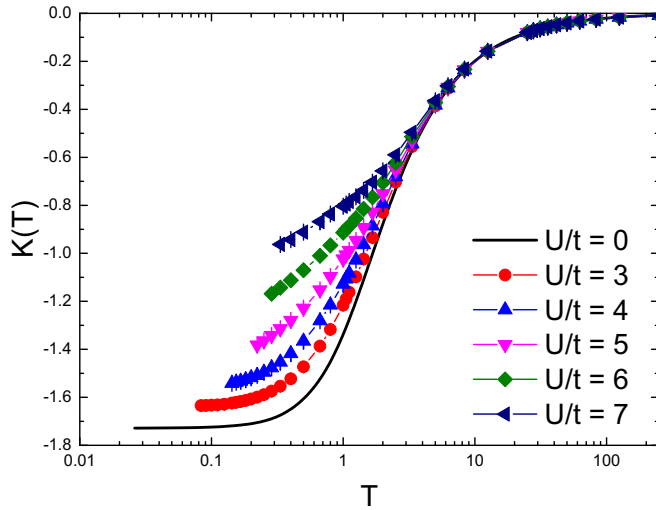


FIG. 9. The average of the kinetic energy term as a function of the temperature for different values of U/t . When not shown, error bars are smaller than the symbol size.

5, $\chi(T)$ has a response similar to the noninteracting case and therefore is consistent with a metallic Pauli paramagnetic state, while for $U/t \gtrsim 6$ it has a monotonically increasing behavior as T decreases (within the temperature range we have analyzed). However, this increase in $\chi(T)$ with decreasing T for large interaction strengths is not enough to define the nature of the spin excitations. The minus-sign problem prevents us from reaching the very low temperatures required to determine whether excitations are gapped or gapless.

D. Transport properties

Finally, we now investigate the transport properties of the system starting with the kinetic energy. Figure 9 displays the kinetic energy per site, $\langle \hat{K} \rangle = -\frac{t}{N} \langle \sum_{(i,j),\sigma} (c_{i\sigma}^\dagger c_{j\sigma} + \text{H.c.}) \rangle$, as a function of temperature for different values of interaction. Since fermionic localization is favored in an insulating state, $\langle \hat{K} \rangle$ has to be reduced as a function of temperature as U increases, a feature noticed in Fig. 9. However, within the temperature scale we investigated, we did not find $\frac{\partial}{\partial T} \langle \hat{K} \rangle < 0$; therefore, different from the analysis of the potential energy, the behavior of the kinetic energy cannot provide clues to the emergence of an insulating phase.

In view of this, other quantities should be investigated to identify the metal-to-insulator transition. Among them, we proceed to examine the fermionic compressibility,

$$\kappa = \frac{1}{n^2} \frac{\partial n}{\partial \mu}, \quad (7)$$

with $n = \frac{1}{N} \langle \sum_{i,\sigma} n_{i\sigma} \rangle$, displayed in Fig. 10(a). Notice that, due to the rotation symmetry, the three orbitals are equivalent, along with their individual compressibilities. When dealing with any degree of anisotropy (of hopping or interaction), it is possible that some orbitals are insulating while others exhibit metallic features, like an orbital-selective Mott phase. However, that is beyond the scope of this work.

For a metallic phase, κ assumes finite values, as presented in Fig. 10(a) for the noninteracting case ($U = 0$). For the in-

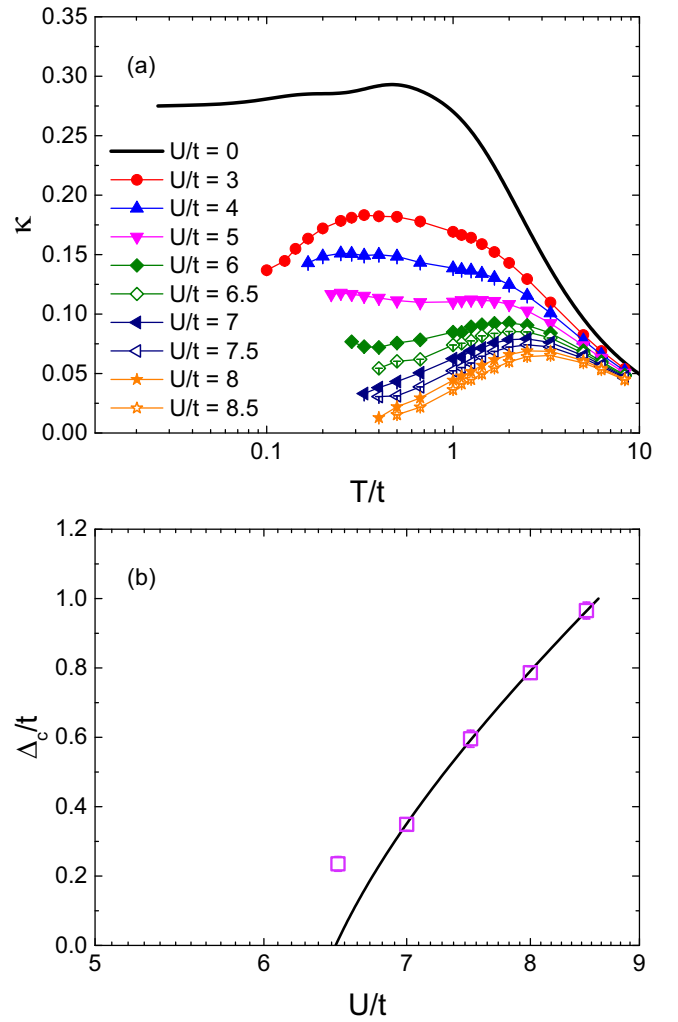


FIG. 10. (a) The electronic compressibility as a function of the temperature for different values of U/t . (b) The charge gap, obtained through the compressibility data, as a function of U/t . When not shown, error bars are smaller than the symbol size.

teracting case, in particular for $U/t \lesssim 5$, the system becomes less compressible, but the trend of κ is still consistent with a metallic phase. Otherwise, for an insulator state, a single-particle gap at the Fermi level of the density of states (DOS) is formed, leading to a plateau in $n(\mu)$ as the temperature is reduced, i.e., to $\kappa \rightarrow 0$. This behavior can be seen for $U/t \gtrsim 6$, where κ has a maximum in a high-temperature scale, followed by an exponential suppression at lower temperatures, as depicted in Fig. 10(a). In other words, there is clear evidence of a metal-to-insulator transition from the behavior of the compressibility.

We further investigate this change in the compressibility for $U/t \gtrsim 6$ by recalling that, within an insulating state, $\kappa \propto \exp(-\frac{\Delta_c}{k_B T})$, with Δ_c being the charge/single-particle gap ($k_B \equiv 1$). Then, we obtain Δ_c by an exponential fit of κ for $U/t \geq 6.5$, as displayed in Fig. 10(b). Assuming a second-order phase transition and performing an extrapolation by a polynomial or a power law function for $U/t \geq 7.0$, we obtain the critical point at $U_c/t = 6.5 \pm 0.1$, as shown by the black solid line [40].

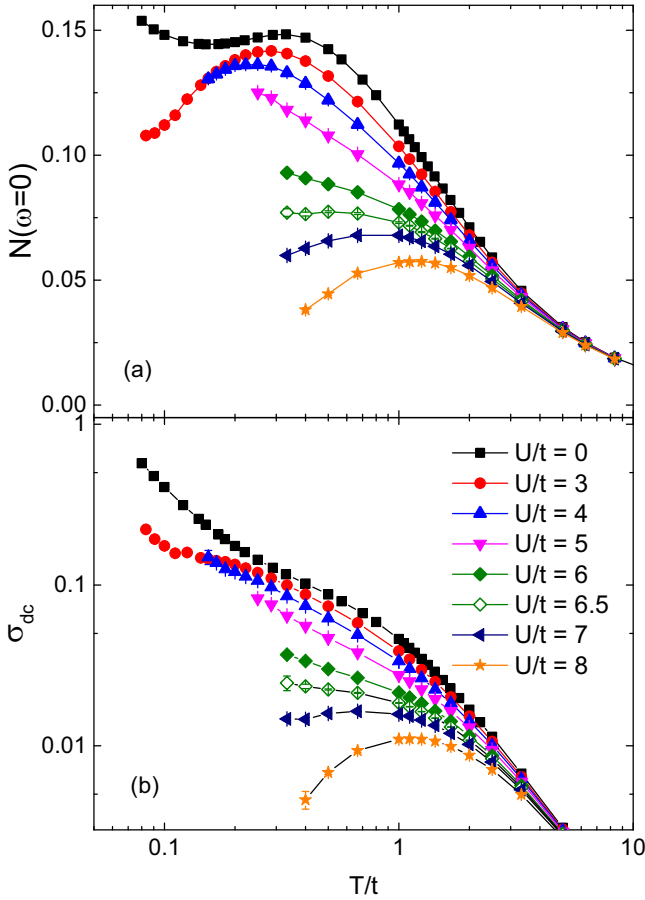


FIG. 11. (a) The density of states at the Fermi level and (b) the dc conductivity as a function of the temperature for different values of U/t . When not shown, error bars are smaller than the symbol size.

At this point, some remarks are required. First, as the charge gap is formed at high temperature for $U/t \geq 7$, we expect that our analysis for Δ_c in Fig. 10(b) has few finite-size effects. Second, we have to recall that, in some circumstances, κ may exhibit unconventional behavior in multiorbital systems, with the charge gap opening only for a few orbitals, while others remain metallic. However, such an orbital-selective Mott transition does not occur in the Hubbard model on the kagome lattice; we have verified that all the orbitals are metallic or insulators.

The previous analysis of κ indirectly points to a suppression of the spectral weight around the Fermi level. Given this, it is important to *directly* probe the DOS as a complementary study. In order to avoid complex methodologies for numerical analytical continuations, here we examine the DOS only at the Fermi level, which is obtained with [41]

$$N(\omega = 0) \approx \frac{\beta}{\pi} G(|\mathbf{i} - \mathbf{j}| = 0, \tau = \beta/2). \quad (8)$$

Figure 11(a) displays $N(\omega = 0)$ as a function of temperature for different values of U/t . Notice that $N(\omega = 0)$ exhibits a finite value for $U/t \lesssim 5$ at low temperatures, consistent with a metallic state. By contrast, for $U/t \gtrsim 6$, the trend of the DOS has a significant change, being reduced exponentially, as expected for an insulator. In particular, within the range

of temperatures examined, the change in behavior occurs at $U/t \approx 6.5$, in very good agreement with the results for the compressibility.

Finally, as further evidence of a metal-to-insulator transition we examine the dc conductivity,

$$\sigma_{dc} = \frac{\beta^2}{\pi} \Lambda_{xx}(\mathbf{q} = \mathbf{0}, \tau = \beta/2), \quad (9)$$

in which

$$\Lambda_{xx}(\mathbf{q}, \tau) = \langle j_x(\mathbf{q}, \tau) j_x(-\mathbf{q}, 0) \rangle, \quad (10)$$

with $j_x(\mathbf{q}, \tau)$ being the Fourier transform of the unequal-time current-current correlation functions

$$j_x(\mathbf{i}, \tau) = e^{\tau \mathcal{H}} \left[it \sum_{\sigma} (c_{\mathbf{i}+\mathbf{x}\sigma}^{\dagger} c_{\mathbf{i}\sigma} - c_{\mathbf{i}\sigma}^{\dagger} c_{\mathbf{i}+\mathbf{x}\sigma}) \right] e^{-\tau \mathcal{H}} \quad (11)$$

(see, e.g., Refs. [42–44]). Figure 11(b) exhibits the results for σ_{dc} as a function of temperature for different values of U/t . Similar to the previous analyses, a metallic behavior, i.e., $\partial \sigma_{dc} / \partial T < 0$, occurs only for $U/t \lesssim 6.5$. For interaction strength larger than that, the behavior is consistent with an insulator.

In summary, the analyses of the compressibility, the DOS at the Fermi level, and the dc conductivity provide strong evidence for a metal-to-insulator transition at $U_c/t = 6.5 \pm 0.5$.

E. Finite-size effects

In this section, we investigate finite-size effects. To this end, we perform simulations for an $N = 10 \times 10$ lattice (i.e., with 300 sites), fixing $U/t = 6$ while varying temperature. Figures 12(a)–12(d) display the total energy, the kinetic energy, the double occupancy, and nearest-neighbor spin-spin correlation functions for this system size, respectively, in comparison with our previous results for $N = 6 \times 6$. Notice that, for these quantities, finite-size effects may be disregarded within the range of temperature examined. Indeed, short-range quantities must suffer much less from finite-size effects than long-range quantities, such as structure factors or susceptibilities. Concerning the latter, next-nearest-neighbor spin correlation functions and the homogeneous magnetic susceptibility exhibit a small dependence on the lattice size at low temperatures, as shown in Figs. 12(e) and 12(f), respectively. However, these minor dependences do not affect the main results discussed in the previous sections.

IV. CONCLUSIONS

In this work, we have investigated thermodynamic, magnetic, and transport properties of the repulsive Hubbard model on the kagome lattice through unbiased DQMC simulations. For the thermodynamic properties, we examined the entropy for different interaction strengths and the behavior of the isentropic curves as a function of U/t . We have found that adiabatic cooling is possible for entropies smaller than $s \approx \ln 2$. In addition, we examined the specific heat: in contrast to what is seen in the Hubbard model in the square or honeycomb lattices, the low-temperature peak seems to be suppressed in the kagome lattice for all U/t . This suggests the absence of collective spin-wave excitations as temperature is reduced,

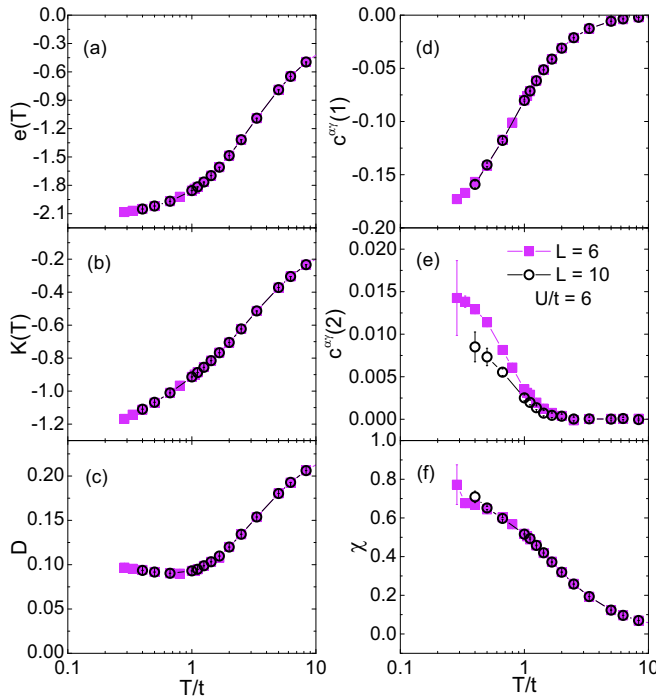


FIG. 12. Comparison between results obtained for 6×6 (solid squares) and 10×10 (open circles) lattices for (a) the total energy, (b) the kinetic energy, (c) the double occupancy, (d) nearest-neighbor and (e) next-nearest-neighbor spin-spin correlation functions, and (f) homogeneous susceptibility as a function of the temperature at $U/t = 6$. When not shown, error bars are smaller than the symbol size.

i.e., the absence of magnetic long-range order in the ground state.

In view of this, we investigated the spin-spin correlation functions, in particular the local moment, nearest neighbors (NNs), and next-nearest neighbors (NNNs). We obtained well-formed local moments, with strong short-range NN correlations functions, while the NNN (and farther) ones are strongly suppressed, further evidencing the absence of magnetic long-range order. Despite this, the homogeneous magnetic susceptibility $\chi(T)$ still increases as temperature is reduced and is enhanced for larger values of U/t . However, we are not able to conclude whether the nature of the spin excitations is gapped or gapless. Furthermore, it is worth mentioning that identifying whether a spin liquid state emerges or not is challenging and beyond the scope of this work.

Finally, we probed the metal-to-insulator transition. In particular, the behavior of the compressibility provides a clear distinction between metallic and insulating states. Therefore, we investigated the behavior $\kappa(T)$ for different values of U/t

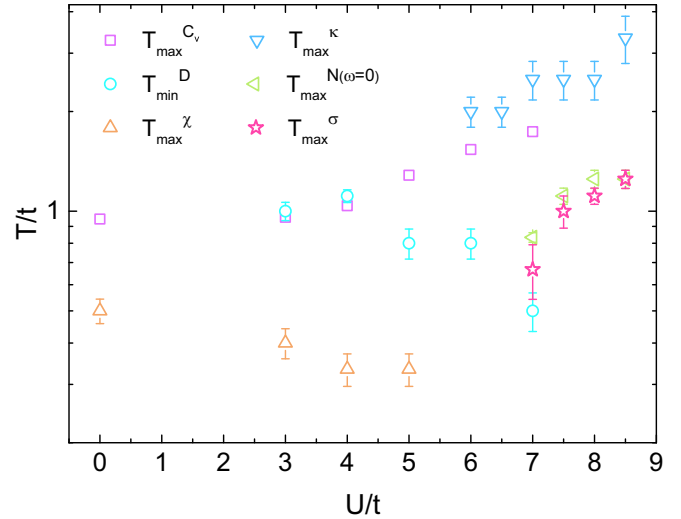


FIG. 13. Different energy scales for the Hubbard model on the kagome lattice for several values of U/t .

and were able to identify the critical point around $U_c/t \approx 6.5$. As complementary analyses, we also examined the DOS at the Fermi level, as well as the current-current correlation functions, leading to results in line with those for the compressibility. Together, these analyses provide clear evidence of a Mott transition at $U_c/t = 6.5 \pm 0.5$.

In summary, our work presented detailed finite-temperature analyses for the Hubbard model in the kagome lattice, allowing us to provide different energy scales of the system. To this end, Fig. 13 presents (i) the minima of the double occupancy T_{\min}^D , as well as the high-temperature maxima for (ii) the specific heat peak T_{\max}^C , (iii) the magnetic susceptibility T_{\max}^χ , (iv) the compressibility T_{\max}^κ , (v) the DOS at Fermi level T_{\max}^N , and (vi) the dc conductivity T_{\max}^σ . Together, Figs. 5 and 13 provide a broad description of the model that could be relevant for future cold atom experiments.

ACKNOWLEDGMENTS

We are grateful to J. P. de Lima for his contributions in the initial stage of this work and to E. C. Andrade for illuminating discussions and suggestions. Financial support from the Brazilian Agencies CAPES, CNPq, FAPERJ, and Instituto Nacional de Ciência e Tecnologia de Informação Quântica (CNPq INCT-IQ 465469/2014-0) is gratefully acknowledged. N.C.C. acknowledges financial support from CNPq, Grant No. 313065/2021-7, and from FAPERJ – Fundação Carlos Chagas Filho de Amparo à Pesquisa do Estado do Rio de Janeiro –, Grant No. E-26/200.258/2023 (SEI-260003/000623/2023).

- [1] J. S. Helton, K. Matan, M. P. Shores, E. A. Nytko, B. M. Bartlett, Y. Yoshida, Y. Takano, A. Suslov, Y. Qiu, J.-H. Chung, D. G. Nocera, and Y. S. Lee, *Phys. Rev. Lett.* **98**, 107204 (2007).
 [2] J. S. Helton, K. Matan, M. P. Shores, E. A. Nytko, B. M. Bartlett, Y. Qiu, D. G. Nocera, and Y. S. Lee, *Phys. Rev. Lett.* **104**, 147201 (2010).

- [3] T.-H. Han, J. S. Helton, S. Chu, D. G. Nocera, J. A. Rodriguez-Rivera, C. Broholm, and Y. S. Lee, *Nature (London)* **492**, 406 (2012).
 [4] M. Fu, T. Imai, T.-H. Han, and Y. S. Lee, *Science* **350**, 655 (2015).
 [5] M. R. Norman, *Rev. Mod. Phys.* **88**, 041002 (2016).

- [6] S. Kempkes, M. Slot, J. van Den Broeke, P. Capiod, W. Benalcazar, D. Vanmaekelbergh, D. Bercioux, I. Swart, and C. Morais Smith, *Nat. Mater.* **18**, 1292 (2019).
- [7] S. Sun, S. Zhao, Y. Z. Luo, X. Gu, X. Lian, A. Tadich, D.-C. Qi, Z. Ma, Y. Zheng, C. Gu, J. L. Zhang, Z. Li, and W. Chen, *Nano Lett.* **20**, 5583 (2020).
- [8] G.-B. Jo, J. Guzman, C. K. Thomas, P. Hosur, A. Vishwanath, and D. M. Stamper-Kurn, *Phys. Rev. Lett.* **108**, 045305 (2012).
- [9] T. H. Barter, T.-H. Leung, M. Okano, M. Block, N. Y. Yao, and D. M. Stamper-Kurn, *Phys. Rev. A* **101**, 011601(R) (2020).
- [10] T.-H. Leung, M. N. Schwarz, S.-W. Chang, C. D. Brown, G. Unnikrishnan, and D. Stamper-Kurn, *Phys. Rev. Lett.* **125**, 133001 (2020).
- [11] S. Yan, D. A. Huse, and S. R. White, *Science* **332**, 1173 (2011).
- [12] Y. Iqbal, F. Becca, S. Sorella, and D. Poilblanc, *Phys. Rev. B* **87**, 060405(R) (2013).
- [13] A. Yamada, K. Seki, R. Eder, and Y. Ohta, *Phys. Rev. B* **83**, 195127 (2011).
- [14] R. Higa and K. Asano, *Phys. Rev. B* **93**, 245123 (2016).
- [15] T. Ohashi, N. Kawakami, and H. Tsunetsugu, *Phys. Rev. Lett.* **97**, 066401 (2006).
- [16] S. Kuratani, A. Koga, and N. Kawakami, *J. Phys.: Condens. Matter* **19**, 145252 (2007).
- [17] N. Bulut, W. Koshibae, and S. Maekawa, *Phys. Rev. Lett.* **95**, 037001 (2005).
- [18] J. Kaufmann, K. Steiner, R. T. Scalettar, K. Held, and O. Janson, *Phys. Rev. B* **104**, 165127 (2021).
- [19] R.-Y. Sun and Z. Zhu, *Phys. Rev. B* **104**, L121118 (2021).
- [20] C. Wen, X. Zhu, Z. Xiao, N. Hao, R. Mondaini, H. Guo, and S. Feng, *Phys. Rev. B* **105**, 075118 (2022).
- [21] A. J. Kim, F. Simkovic, and E. Kozik, *Phys. Rev. Lett.* **124**, 117602 (2020).
- [22] R. Blankenbecler, D. J. Scalapino, and R. L. Sugar, *Phys. Rev. D* **24**, 2278 (1981).
- [23] J. E. Hirsch, *Phys. Rev. B* **28**, 4059 (1983).
- [24] J. E. Hirsch, *Phys. Rev. B* **31**, 4403 (1985).
- [25] S. R. White, D. J. Scalapino, R. L. Sugar, N. E. Bickers, and R. T. Scalettar, *Phys. Rev. B* **39**, 839 (1989).
- [26] R. R. dos Santos, *Braz. J. Phys.* **33**, 36 (2003).
- [27] F. Assaad, in *Quantum Simulations of Complex Many-Body Systems: From Theory to Algorithms*, edited by J. Grotendorst, D. Marx, and A. Muramatsu, NIC Series, Vol. 10 (John von Neumann Institute for Computing, Jülich, Germany, 2002), pp. 99–156.
- [28] J. Gubernatis, N. Kawashima, and P. Werner, *Quantum Monte Carlo Methods: Algorithms for Lattice Models* (Cambridge University Press, Cambridge, 2016).
- [29] F. Becca and S. Sorella, *Quantum Monte Carlo Approaches for Correlated Systems* (Cambridge University Press, Cambridge, 2017).
- [30] E. Y. Loh, J. E. Gubernatis, R. T. Scalettar, S. R. White, D. J. Scalapino, and R. L. Sugar, *Phys. Rev. B* **41**, 9301 (1990).
- [31] M. Troyer and U.-J. Wiese, *Phys. Rev. Lett.* **94**, 170201 (2005).
- [32] A.-M. Daré, L. Raymond, G. Albinet, and A. M. S. Tremblay, *Phys. Rev. B* **76**, 064402 (2007).
- [33] T. Paiva, R. T. Scalettar, C. Huscroft, and A. K. McMahan, *Phys. Rev. B* **63**, 125116 (2001).
- [34] E. Khatami and M. Rigol, *Phys. Rev. A* **84**, 053611 (2011).
- [35] B. Tang, T. Paiva, E. Khatami, and M. Rigol, *Phys. Rev. Lett.* **109**, 205301 (2012).
- [36] B. Tang, T. Paiva, E. Khatami, and M. Rigol, *Phys. Rev. B* **88**, 125127 (2013).
- [37] T. Paiva, R. T. Scalettar, W. Zheng, R. R. P. Singh, and J. Oitmaa, *Phys. Rev. B* **72**, 085123 (2005).
- [38] T. Paiva, R. Scalettar, M. Randeria, and N. Trivedi, *Phys. Rev. Lett.* **104**, 066406 (2010).
- [39] M. Udagawa and Y. Motome, *Phys. Rev. Lett.* **104**, 106409 (2010).
- [40] Notice that the exponential fitting is not adequate when $\Delta_c \ll T$, which may lead to misleading results. Therefore, it is safe to disregard the point $U/t = 6.5$ when analyzing the extrapolation.
- [41] N. Trivedi and M. Randeria, *Phys. Rev. Lett.* **75**, 312 (1995).
- [42] N. Trivedi, R. T. Scalettar, and M. Randeria, *Phys. Rev. B* **54**, R3756 (1996).
- [43] P. J. H. Denteneer, R. T. Scalettar, and N. Trivedi, *Phys. Rev. Lett.* **83**, 4610 (1999).
- [44] R. Mondaini, K. Bouadim, T. Paiva, and R. R. dos Santos, *Phys. Rev. B* **85**, 125127 (2012).